

## Unstrained islands with interface coincidence sites versus strained islands: X-ray measurements on Ag/ZnO

N. Jedrecy,<sup>1,\*</sup> G. Renaud,<sup>2</sup> R. Lazzari,<sup>1</sup> and J. Jupille<sup>1</sup>

<sup>1</sup>Institut des NanoSciences de Paris, Universités Paris 6 et 7 and CNRS-UMR 7588, 4 Place Jussieu, 75252 Paris Cedex 05, France

<sup>2</sup>CEA-Grenoble, DRFMC/SP2M/NRS, 17 rue des Martyrs, 38054 Grenoble Cedex 9, France

(Received 21 July 2005; revised manuscript received 21 September 2005; published 4 November 2005)

The structure and shape of (111) Ag nanocrystals formed at room temperature on basal ZnO planes is followed *in situ* by synchrotron surface x-ray measurements. On well-ordered surfaces, fully relaxed islands are preferred with their in-plane lattice perfectly aligned with that of the substrate. These islands have their bulk lattice parameter from the earliest stages of the growth. At unit cell scale, the Ag lattice is incommensurate with that of ZnO (−11% lattice mismatch), but interface coincidence sites occur every 2.6 nm. The islands grow with a plateau shape and the height-to-width ratio decreases rapidly with increasing coverage. These features are enhanced on the more ordered surfaces. In the low-coverage regime, small clusters rotated by  $30\pm 3^\circ$  may be found. These minority clusters, in registry with ZnO, grow with the face-centered cubic stacking only on ill-crystallized surfaces. The  $30^\circ$  epitaxial growth is rapidly inhibited due to the stress field generated by the compressive strain (up to −2.6% with respect to bulk Ag) and the interface geometry. It is proposed that the different interface structures result from a subtle metal-oxide interaction potential possibly involving superperiodic lateral variations.

DOI: [10.1103/PhysRevB.72.195404](https://doi.org/10.1103/PhysRevB.72.195404)

PACS number(s): 68.65.-k, 68.55.-a, 68.35.-p, 81.07.-b

### I. INTRODUCTION

Of major interest is the identification of mechanisms that govern the growth of metal films on insulator or semiconductor oxides, in view of the numerous important applications (coatings,<sup>1</sup> supported catalysts,<sup>2,3</sup> magnetic tunnel junctions,<sup>4</sup>...) where metal-oxide systems are involved. In the case of metals on covalent semiconductors, three growth modes are referred to: the layer-by-layer Frank–van der Merwe (FM) mode, the Volmer-Weber (VW) mode with three-dimensional (3D) islands as precursors of the growth, and the Stranski-Krastanov mode where a continuous wetting layer is formed before 3D islanding. Almost all growth studies concerning transition metals on oxide surfaces report on the VW mode.<sup>5,6</sup> One commonly invokes the much greater surface free energy of the metal than that of the oxide. In the context of epitaxy, whatever the growth mode may be, the bulk lattice parameter mismatch (BLPM) magnitude determines the crystalline orientation of the adsorbate and its “coherent”-“incoherent” matching with the substrate.<sup>7,8</sup> The fully coherent state refers to islands or layers elastically strained to the substrate, while the incoherent state refers to islands or layers having their bulk parameter, with or without the occurrence of interface dislocations. Heteroepitaxies associated with a moderate BLPM (<10%) tend to result in highly coincident atomic structures at early growth stage (pseudomorphic regime), the film relaxing towards its regular parameter upon increasing coverage (plastic relaxation regime).

Peculiar wetting behaviors of noble transition metals on basal ZnO planes, both oxygen (000 $\bar{1}$ ) and zinc (0001) terminated, have been reported.<sup>9–11</sup> Copper and silver form (111) oriented two-dimensional (2D) islands, the metal surface hexagonal cell aligning with the ZnO one. For silver, the surface BLPM of −11.1% leads to an almost perfect lattice

coincidence every 9 (8) Ag (ZnO) unit cells. This was suggested to govern the metal growth with its bulk lattice constant.<sup>11</sup> A second epitaxy may be observed<sup>12</sup> where the Ag lattice is rotated by  $30^\circ$  in the surface plane and the BLPM is +2.63%. The interdependence of orientation, stress, and interface size is largely unknown in the VW growth of metal clusters. The present work aims at examining this topic by an *in situ* synchrotron x-ray scattering study of the Ag/ZnO interface.

### II. EXPERIMENTAL DETAILS AND CONVENTIONS

In one case (referred to as *A*), the ZnO substrates were cleaned in UHV by several cycles of Ar<sup>+</sup> ion sputtering, then annealing (>1000 K), followed by subsequent cooling down under O<sub>2</sub> pressure (10<sup>−5</sup>–10<sup>−4</sup> mbar). An optimized procedure consists of performing the bombardments from 2 to 0.6 keV, while annealing up to 1350 K. In the other case (referred to as *B*), the substrates were simply outgassed at 900 K under O<sub>2</sub>. Silver was deposited at room temperature using a Knudsen cell (0.55 Å per min). The x-ray scattering data were collected at the BM32 beam line of the European Synchrotron Radiation Facility (ESRF), by means of a 6-circle diffractometer in the *z*-axis mode. A focused x-ray beam at energy of 18 keV was used, with grazing incidence geometry near the total reflection. Intensities related to surface x-ray diffraction (SXRD) (Refs. 13 and 14) and grazing incidence small-angle x-ray scattering (GISAXS) (Ref. 15) were measured by means of a scintillator detector and a charge-coupled device (CCD) camera, respectively.

The two polar ZnO (0001)-Zn and (000 $\bar{1}$ )-O surfaces are known to stabilize in UHV with the (1 × 1) periodicity of an ideal bulk truncation.<sup>10,16,17</sup> We thus use for describing the surface the lattice vectors of the hexagonal bulk structure, i.e.

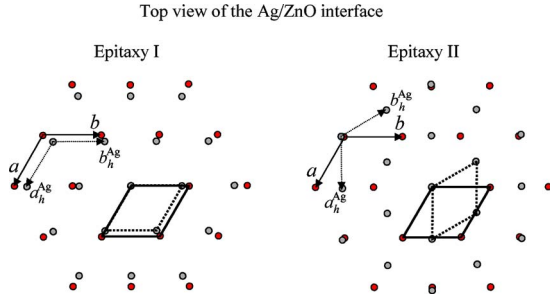


FIG. 1. (Color online) Top views of a Ag (111) atomic layer on top of a ZnO(000 $\bar{1}$ )-O surface layer, according to the two most probable azimuthal orientations. Ag atoms are in light gray, O atoms are in red. The silver in-plane spacing is assumed to be as in the bulk.

( $\mathbf{a}, \mathbf{b}, \mathbf{c}$ ), where  $\mathbf{c}$  is along the surface normal. The Zn surface is characterized by incomplete layers<sup>16,17</sup> but this does not play a significant role in the present study. Silver crystallizes in the face-centered cubic (fcc) structure. Its growth proceeds on ZnO via the (111) layers of hexagonal symmetry. The ( $1 \times 1$ ) surface cell vectors ( $\mathbf{a}_h^{\text{Ag}}, \mathbf{b}_h^{\text{Ag}}, \mathbf{c}_h^{\text{Ag}}$ ) can be written in the cubic basis ( $\mathbf{a}^{\text{Ag}}, \mathbf{b}^{\text{Ag}}, \mathbf{c}^{\text{Ag}}$ ) as  $\mathbf{a}_h^{\text{Ag}} = 1/2[10\bar{1}]$ ,  $\mathbf{b}_h^{\text{Ag}} = 1/2[\bar{1}10]$ ,  $\mathbf{a}_h^{\text{Ag}} = [111]$ . Two orientations of the Ag surface cell ( $\mathbf{c}_h^{\text{Ag}} // \mathbf{c}$ ) may *a priori* be considered (see Fig. 1). In the epitaxy referred to as I, the ZnO and Ag surface cells are parallel and the BLPM  $[(a - a_h^{\text{Ag}})/a]$  is equal to  $-11.1\%$  (we take as bulk lattice constants  $a = b = 3.25 \text{ \AA}$ ,  $c = 5.207 \text{ \AA}$ , and  $a^{\text{Ag}} = b^{\text{Ag}} = c^{\text{Ag}} = 4.0853 \text{ \AA}$ ). The epitaxy referred to as II reverts to turn the previous silver cell by  $30^\circ$  around  $\mathbf{c}([10\bar{1}]^{\text{Ag}} // [210]^{\text{ZnO}})$ . Considering the Ag ( $2 \times 2$ ) and ZnO ( $\sqrt{3} \times \sqrt{3}$ )R $30^\circ$  surface cells, the BLPM  $[(a - 2a_h^{\text{Ag}}/\sqrt{3})/a]$  is  $+2.63\%$  along the closest-packed atomic rows of Ag, which align between those of ZnO. Any scattering event is referred to by use of the coordinates ( $h, k, \ell$ ) in the ZnO reciprocal lattice basis ( $\mathbf{a}^*, \mathbf{b}^*, \mathbf{c}^*$ ) of the vector  $\mathbf{q} = (\mathbf{k}_f - \mathbf{k}_i)/(2\pi)$ , where  $\mathbf{k}_i$  and  $\mathbf{k}_f$  stand for the incident and scattered x-ray wave vectors, respectively ( $k_i = k_f = 2\pi/\lambda$ ,  $\lambda$  is the wavelength). Silver Bragg reflections are specified using the standard cubic notation. Due to the semi-infinite nature of the ZnO crystal, the coordinate  $\ell$  acts as a continuous variable.<sup>18</sup> We will use the so-called crystal truncation rod (CTR) appellation to design a rod of intensity at ( $h, k$ ) position. Figure 2 shows the reciprocal lattice at  $\ell = 0$  expected from epitaxies I and II, Ag and ZnO being in their bulk state. Open circles locate the Ag CTRs which may arise from crystallites with semi-infinite character. The morphological-structural-strain state of silver is derived from x-ray intensity profiles, performed along specific in-plane (at fixed  $\ell$ ) or out-of-plane [at fixed ( $h, k$ )] directions. The surface coherent domain size (CDS) of ZnO, derived from rocking scans at  $\ell = 0.5$  [ $\text{CDS} = 1/(q_{\parallel} \Delta\omega)$ , where  $\Delta\omega$  is the angular width] ranges from 300 to 1300  $\text{\AA}$  for samples A, and is about 60  $\text{\AA}$  for samples B. Given the good bulk crystalline quality of the ZnO samples, the CDS yields the terrace size. Hence, one may distinguish between smooth (A) and rough (B) surfaces. A nominal thickness of 1  $\text{\AA}$  of Ag corresponds to 0.4 monolayer (ML).

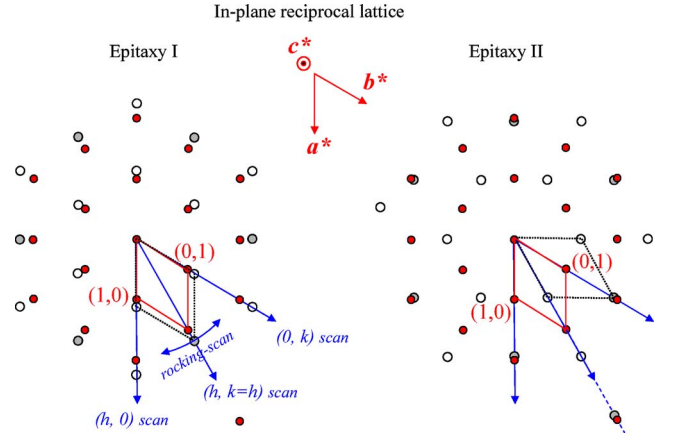


FIG. 2. (Color online) The reciprocal space in the plane of the surface ( $\ell \sim 0$ ), according to epitaxies I and II with bulklike lattice parameter. ZnO (Ag) Bragg reflections are indicated by red (light gray) filled circles. The position of Ag CTRs is indicated by empty circles.

### III. RESULTS AND DISCUSSION

#### A. The hexagon-on-hexagon epitaxy I

For Ag bulklike crystallites in epitaxy I, one expects the  $02\bar{2}$  Bragg reflection to occur at  $h = 1.125$  in an ( $h, h$ ) scan performed in the surface plane ( $\ell = 0.1$ ). For epitaxy II, the same reflection is expected in an ( $h, 0$ )-type scan at  $h = 1.948$ . For all samples, in-plane Ag signals could be measured, at any stage of the growth, at the right side of the ZnO (1,1) CTR, whereas no signal could be detected in the tail of the ZnO (2,0) CTR. Epitaxy I is thus the dominant epitaxy whatever the surface termination (O or Zn) or its crystalline quality may be. Moreover, the Ag in-plane lattice parameter, from the very first stages ( $> 0.17$  ML), is that expected from bulk to within  $0.26$ – $0.44\%$ . Figures 3(a) and 3(b) show typical in-plane profiles as they may be obtained starting from surfaces with a CDS  $\sim 900 \text{ \AA}$ . For the 4  $\text{\AA}$  (1.7 ML) coverage, the profile fit provides a peak center value  $h = 1.128$ . This gives, with respect to silver in bulk, a lattice parameter contraction in the plane of the interface of only  $-0.26\%$ . Upon increasing coverage, the lattice parameter slowly evolves towards its exact bulk value, which is reached after 100  $\text{\AA}$  of Ag has been deposited. Taking the magnitude of the BLPM into account ( $-11.1\%$ ), the deviation from bulk state, though detectable up to 32 ML, is of trifling amount. It is worth noticing the lattice parameter does not evolve in accordance with the BLPM sign. Interface stress and confinement effects could be at the origin of the small residual compressive strain. The next allowed Bragg reflection at ( $h, k$ ) = (1.125, 1.125) is expected to occur for  $\mathbf{q}_z = 3\mathbf{c}_h^{\text{Ag}*}$ , that is at  $\ell = 2.208$ . At least three (111) MLs with fcc stacking sequence are required to produce this out-of-plane  $13\bar{1}$  peak, visible as soon as 1  $\text{\AA}$  has been deposited [Fig. 3(c)]. The fit of the  $\ell$ -profile for 4  $\text{\AA}$  of Ag leads to the value  $\ell = 2.214$ , which is a contraction of the (111) interlayer spacing with respect to bulk equal to  $-0.26\%$ . The bulk distance is reached for 24  $\text{\AA}$  of Ag. As for the 1  $\text{\AA}$  amount, the islands

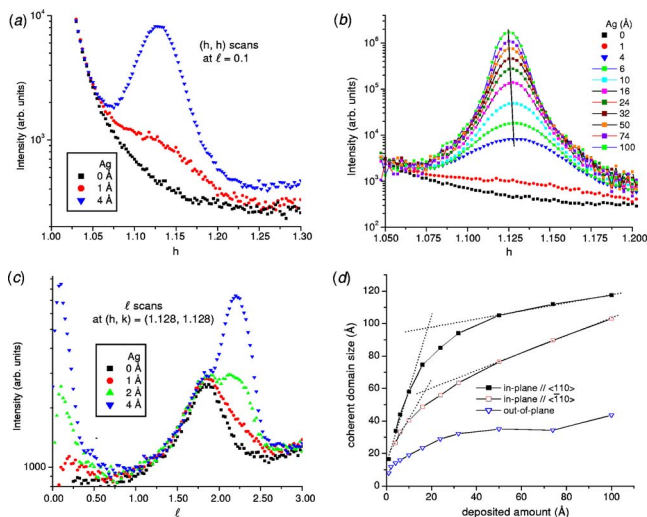


FIG. 3. (Color online) The in-plane (a), (b) and out-of-plane (c) x-ray profiles recorded for different deposited amounts of Ag on samples of type A. The Ag signals relate to epitaxy I with a lattice parameter very close to the bulk one. The 4 Å (1.7 ML) coverage gives a lattice constant that deviates by less than  $-0.26\%$  from the bulk one, the latter being reached for 100 Å of Ag. (d) Ag coherent domain size values derived from the x-ray signals.

seem slightly expanded by  $+0.9\%$  along the normal. Substrate-induced displacements of Ag atoms in the first layer, perpendicular to the interface plane, are presumably responsible for this observation.

The above results are quite surprising. On the one hand, the exact alignment (verified by means of rocking scans) of the Ag closest-packed rows with the ZnO rows points towards preferential adsorption sites. On the other hand, the Ag lattice parameter strongly differs from that of the oxide. One may wonder if the small strain ( $-0.26\%$ ) does not arise from averaging over parts being compressed in-plane (up to  $-11\%$ ) and other parts being expanded (up to  $+11\%$ ). In the case of islands, the signal width is mainly determined by the finite size. Besides, the  $h$  spreading of the Ag signal gives first-neighbor distances differing by at most  $\pm 7\%$  from the bulk lattice constant. It is more realistic to conclude that lattice spacing is close to bulk. We mention here that the ZnO CTRs have been measured at each step of the growth. The changes with respect to the clean surface<sup>10</sup> are negligible (within the error bar derived from the counting statistics and the reproducibility of equivalent reflections). Adatom-adatom lateral interactions thus prevail over adatom-substrate interactions from the earliest stages of the growth. The perfect alignment of the unstrained islands could be driven by the moiré superstructure depicted in Fig. 4. Indeed, the lattice mismatch of a  $9 \times 9$  bulklike Ag surface cell with respect to an  $8 \times 8$  ZnO cell amounts to only  $-0.0065\%$ . Islands may be pinned to the substrate by alternations of Ag atoms every 8 ZnO top site and/or every 8 bridge-hcp-fcc site. Any interfacial stress in mismatching zones [unfavorable location of some adatoms within the  $(8 \times 8)$  cell] is compensated by the metal cohesive energy (bulk spacing). The quasiperfect coincidence relation concerns islands with a minimal side length of 2.6 nm, but high-symmetry Ag/ZnO

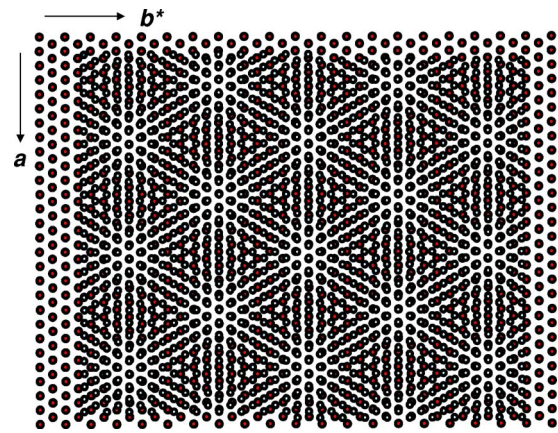


FIG. 4. (Color online) Moiré schematic top view of the Ag/ZnO interface, involving Ag (111) and ZnO (0001) atomic planes, with their in-plane bulk spacing and alignment of the closest-packed rows (epitaxy I).

atomic configurations are already present in half-sized islands.

### B. The growth mode of islands of type I

Estimates of silver in-plane CDSs ( $\sim 1/\Delta q_{\parallel}$ , where  $\Delta q_{\parallel}$  is the signal width) along  $(a+b)$  and along  $(-a+b)$  were obtained from radial and transverse rocking scans, respectively, across  $(h, k, \ell) = (1.128, 1.128, 0.1)$ . The values (confirmed by scans performed at  $\ell = 2.2$ ) for the ZnO-O surface with CDS  $\sim 900$  Å are reported as a function of the coverage in Fig. 3(d). First, a higher degree of crystallinity is achieved along  $[110]^{\text{ZnO}}$  than along  $[\bar{1}10]^{\text{ZnO}}$ . In the 0–20 Å coverage range, the ratio between the two CDSs stays close to the ratio ( $\sqrt{3}$ ) between lattice units along the two axes. Second, two growth regimes may be identified. In-plane crystalline order rapidly improves up to 20 Å (8.5 ML) of deposited amount. It follows a much slower linear progression in the high coverage range [ $>40$  Å (17 ML)]. In the 0–20 Å growth regime, the CDS may be assimilated to the island size. The preferred lateral growth in the very first stages is confirmed by the higher increase of the in-plane CDS with respect to the out-of-plane CDS ( $\sim 1/\Delta q_{\perp}$ ). It is also consistent with the fact that islands rapidly adopt (2 Å of Ag) a plateau shape with (111) top terraces, as demonstrated by the diffuse x-ray scattering measured by means of rocking scans across the  $(h, k) = (1.125, 0)$  rod, far from Bragg reflections (for instance at  $\ell = 0.1$ ). The roughness parameter  $\beta$  (Ref. 18) is estimated equal to 0.4 for 8 Å of Ag. Concerning the (111) stacking sequence, the two fcc variants, i.e., ABC or ACB, are rapidly (8 Å) in close proportion. For an ACB stacking, Bragg reflections are expected at  $\mathbf{q}_z = 1(2)c_h^{\text{Ag}^*}$ , then  $4(5)c_h^{\text{Ag}^*}$  along rods of type  $(1, 0)$   $[(-1, 0)]$ . We measure the same intensities every  $60^\circ$  (instead of  $120^\circ$ ) rotation about  $c$ . Terraces rotated by  $60^\circ$  are equal on the clean ZnO surfaces.<sup>16</sup> The two stacking sequences may be determined by the distinct terrace orientations, or involve twinned grains inside the islands.<sup>19</sup> This would explain why the Ag CDS reaches limiting values both along the normal and in the surface plane.

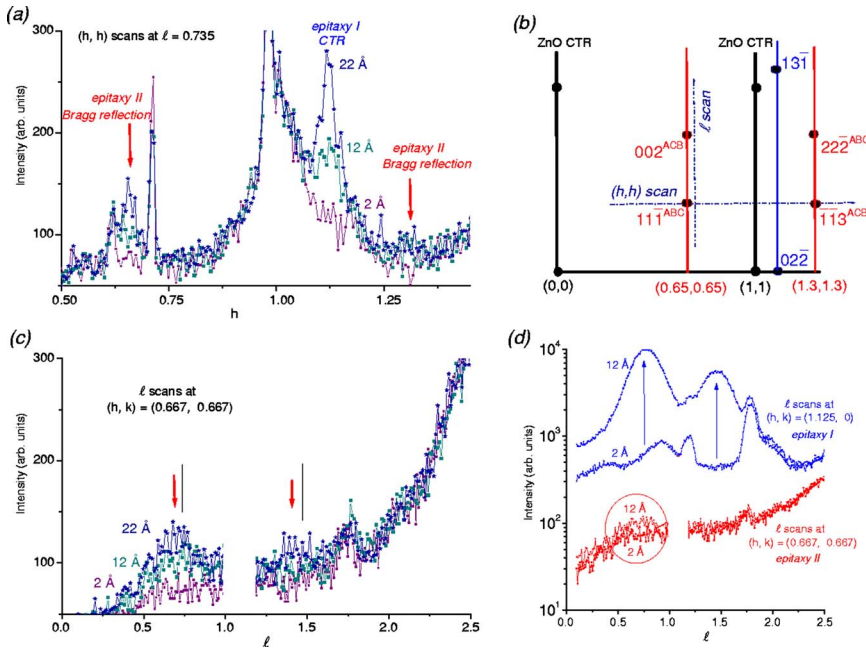


FIG. 5. (Color online) The in-plane (a) and out-of-plane (c), (d) x-ray profiles recorded for different deposited amounts of Ag on samples of type *B*. Signals related to either the epitaxy I or the epitaxy II may be observed. In (c), arrows and vertical lines indicate positions related to islands II, elastically strained with respect to ZnO or bulklike, respectively. (b) Cut view of the reciprocal space.

Unstrained flat-top islands have also been observed in the Cu/ZnO case, where the bulk lattice constants are compatible with a Ag(5×5)/ZnO(4×4) moiré superstructure.<sup>10</sup> Pillarlike shapes have been related to fully relaxed incoherent islands.<sup>20</sup> The specificity of copper and silver on ZnO is that they both grow with enhanced 2D character in the VW mode. The kinetics and energetics of adatom migration have been considered to explain the nearly 2D growth of Cu/ZnO at 130 K.<sup>9,21</sup> At 300 K, the thinnest Cu or Ag islands involve more than one ML [at least three for 0.4 Å of Ag] and the growth process is certainly complex, involving adatom diffusion, island nucleation, up-down edge diffusion, cluster diffusion, coalescence, ...<sup>22,23</sup> Without discounting kinetics, one may speculate that the Ag island lateral extension is thermodynamically favored by the coincidence superstructure, which should result in a subtle balance between short-range adsorbate-adsorbate and/or adsorbate-oxide interactions and longer-range interactions. Local variations of the potentials seen by electrons within the islands are expected, periodically reproduced every 8 ZnO unit cells.

The strain is only  $-0.26\%$  for an in-plane width of the same order of magnitude as the (9×9) supercell width ( $\sim 26$  Å). The bulk state (0% strain) is reached for a size slightly larger than 4 supercells ( $\sim 100$  Å), from which the upper crystallinity regime begins. As soon as 26 Å wide precursor islands have been formed (4 Å coverage), “layer-by-layer” growth may proceed on top without 3D shapes or side facets needed to develop. However, up to a critical amount of 20 Å, the layers grow mostly laterally, a critical island size ( $\sim 100$  Å) being needed before subsequent layers grow on top equally. The transition from the lateral towards the pseudo-layer-by-layer growth is delayed for less ordered surfaces (30 Å of deposited amount instead of 20 Å, starting from 300 Å wide ZnO domains instead of 900 Å). As for the chemical nature of the bare surface, it does not noticeably act on the Ag crystalline order, whereas a higher sticking coefficient of Ag on the O face than on the Zn face has been

reported.<sup>11</sup> This is not surprising since perturbations in the long-range order are unavoidable in a nucleation-coalescence growth process.

### C. The 30° rotated epitaxy II

If ZnO is simply annealed at moderate temperature (samples *B*), one detects the epitaxy II coexisting with the epitaxy I in the low coverage regime. For epitaxy I, scanning parallel to  $(\mathbf{a}^* + \mathbf{b}^*)$  reverts to scanning parallel to  $(\mathbf{a}_h^{\text{Ag}^*} + \mathbf{b}_h^{\text{Ag}^*})$ . For epitaxy II, this reverts to scanning parallel to  $\mathbf{a}_h^{\text{Ag}^*}$ . Figure 5(a) shows such scans performed at  $\mathbf{q}_z = c_h^{\text{Ag}^*} = 0.736 c^*$  for different Ag coverages on a ZnO-Zn surface with CDS  $\sim 56$  Å. One successively crosses [Fig. 5(b)] the  $11\bar{1}$  Bragg reflection relative to epitaxy II with ACB stacking, the ZnO CTR, the Ag CTR relative to epitaxy I, and the  $1\bar{1}3$  Bragg reflection relative to epitaxy II with ABC stacking. Notice that the proportion of Ag islands in epitaxy II with respect to those in epitaxy I is very weak, since the intensity of  $11\bar{1}$  from epitaxy II is lower than that across the CTR from epitaxy I. Moreover, the growth of type II is clearly not favored [see the equivalent (1,0)-type CTRs in Fig. 5(d)], the ratio between islands II and I being about 3% for 12 Å of Ag. A reliable determination of the Ag in-plane lattice parameter requires scanning at  $\ell \sim 0$ . Unfortunately, the in-plane node  $02\bar{2}$  from epitaxy II is located either exactly at the position of the (2, 0) ZnO CTR (full accommodation), or in close vicinity (Ag bulk state). We never could detect it. Considering the out-of-plane reflection  $11\bar{1}$ , a bulk parameter should induce in an  $(h, h)$  scan a peak centered on  $h=0.6495$ . The matching of Ag with ZnO, that is a compression of the Ag surface unit cell by  $-2.63\%$  with respect to bulk, should lead to  $h=0.667$ . The  $11\bar{1}$  reflection is found at  $h=0.66$ , indicating the compressive in-plane state is not total ( $-1.63\%$  vs  $-2.63\%$ ). However, the out-of-plane position is  $\ell=0.7$  (the 002 reflection being accordingly found at  $\ell=1.4$ ),

and this even after 22 Å have been deposited [Fig. 5(c)]. This provides a (111) interlayer distance of 2.48 Å, in comparison with 2.3586 Å for bulk. The out-of-plane expansion of 5.15% compares nicely with the 5.35% value expected from a full elastic accommodation of Ag on top of ZnO. We conclude that the Ag (111) planes with orientation II are in registry with ZnO at the interface, a partial in-plane relief taking place in the upper layers. In the 10–20 Å coverage range, the in-plane crystallinity of islands II looks similar to that of islands I, but the ZnO surface CDS is herein only 56 Å, preventing lateral extension of islands I (40 Å instead of 80 Å). Nevertheless, islands I grow at the expense of islands II, and they are soon an overwhelming majority. Reports on systems involving coherent islands coexisting with incoherent islands are scarce, but the much slower growth of strained clusters with respect to relaxed ones has been observed<sup>20</sup> by scanning tunneling microscope (STM). It has tentatively been described on the basis of elastic energy calculations.<sup>23</sup>

Islands with the in-plane orientation II, but without any out-of-plane order, are sometimes detected (not systematically) on well-crystallized surfaces. Figure 6(a) shows an  $(h, h)$  scan performed at  $\ell=0.1$  and concerning 10 Å of Ag on ZnO-O (CDS  $\sim 900$  Å). At the right side of the 02 $\bar{2}$  peak from epitaxy I, a signal centered on  $h=1.33$  (islands II elastically strained to ZnO) with a small bump at  $h=1.3$  (bulk-like islands II) is measured. For more than three fcc-stacked (111) planes, a Bragg peak would have been expected at  $\ell \sim 0.73$ , whereas the (1.3,1.3,0.1) profile is featureless. To ensure the epitaxial relationship is Ag(111)//ZnO(0001) with  $a_h^{Ag} // (a+b)$ , we have performed a large rocking scan across (1.3,1.3,0.1) [Fig. 6(b)]. The signal decomposes into two components at  $\pm 3^\circ$  from the position related to a perfect alignment of Ag rows with  $[110]^{ZnO}$  and is entirely reproduced at  $\pm 60^\circ$ . The poor crystallinity ( $\sim 8.4$  Å), together with the main disorientations by  $\pm 3^\circ$ , point towards the unfavorable interface energy of the epitaxy II, which is stabilized only over short distances (possibly at ZnO steps and/or ledges). Clusters of type II may also change their orientation with increasing size.<sup>24</sup>

#### D. Epitaxy II versus epitaxy I—Discussion

We observe either 2D-shaped islands (17–110 Å side length) perfectly aligned with the ZnO lattice axes and fully relaxed, or clusters (8–40 Å side length) rotated by  $30 \pm 3^\circ$  and strained with respect to the substrate. The second type of islands grows in height only on ill-crystallized surfaces. It is important to notice that the low BLPM of epitaxy II allows for the formation of small clusters under compressive strain, while the important BLPM of epitaxy I leads to bulklike islands. It is inferred that the equilibrium structure and orientation of the vapor-deposited islands are determined by competing short-range bonding and longer-range interactions. On short distances ( $< 56$  Å), adsorbate-adsorbate interactions are in balance with adsorbate-oxide interactions, and both epitaxies I and II may occur. On longer distances ( $> 56$  Å), only islands with the orientation I develop. The adsorbate-substrate-interaction potential is expected to be

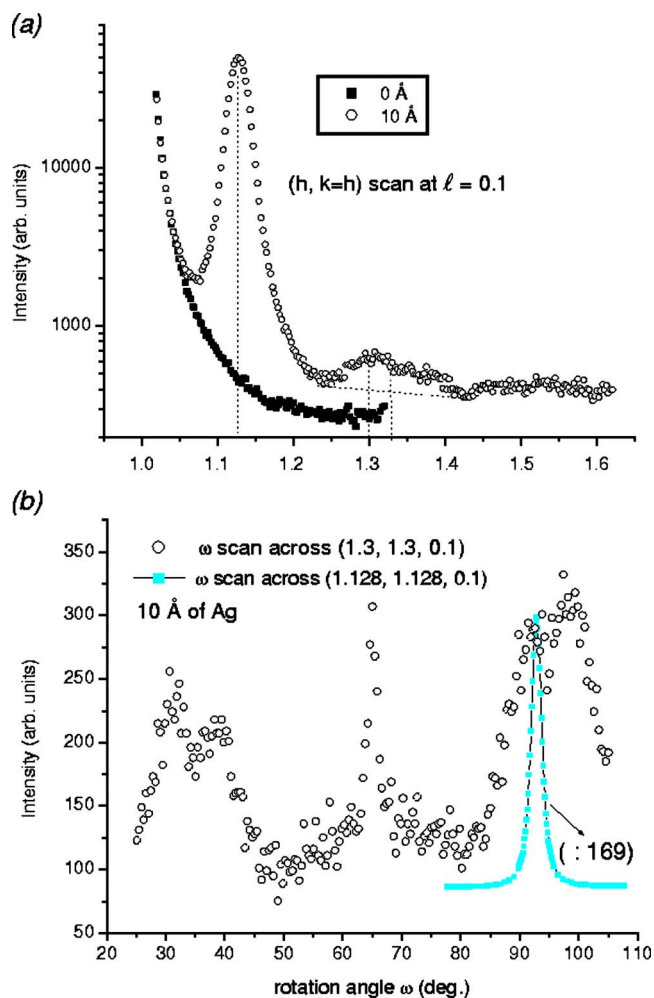


FIG. 6. (Color online) (a) In-plane radial profiles recorded before and after 10 Å of Ag have been deposited on a ZnO sample of type A. The signals (indicated by dotted lines) at  $h=1.33$  and 1.3 are expected for silver islands with the orientation II, either strained with respect to ZnO or fully relaxed, respectively. (b) In-plane rocking-scans performed across each Ag signal seen in (a) (at  $h=1.128$  concerning orientation I and at  $h=1.3$  concerning orientation II).

strongly modified by the coincidence superstructure every 8 ZnO (9 Ag) unit cells. One could question why no transition towards incoherent state is observed with the orientation II. The low BLPM is a handicap here since it does not induce any superlattice coincidence. Also, the closest-packed rows of Ag atoms are just between the O (or Zn) rows, a geometry which is thermodynamically less favorable than geometry I in the bulk spacing assumption.

Superstructures in STM corrugation patterns have been observed in a number of interfaces. Some concern the FM growth of noble metals on metal surfaces,<sup>25,26</sup> the others concern the growth of thin oxide films.<sup>27–30</sup> In metal-metal systems, different moiré patterns may occur as a function of the lattice strain relaxation,<sup>25</sup> at the expense of interface energy (metallic binding). Moiré patterns similar to that in Fig. 4 have been seen on two oxide-metal systems involving, as Ag/ZnO, a BLPM of about 10%.<sup>27,30</sup> Theoretical investigations on metal-oxide interfaces have up to now focused on

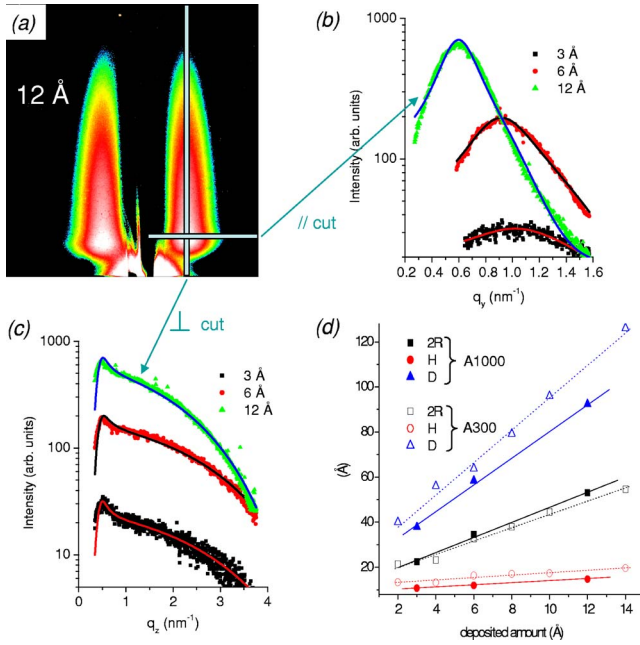


FIG. 7. (Color online) (a) A typical 2D GISAXS intensity pattern (12 Å of Ag) obtained from a sample with a ZnO surface coherent domain size about 1000 Å. (b), (c) Intensity profiles extracted from several 2D GISAXS patterns and related to the same sample. (d) The in-plane size ( $2R$ ), height ( $H$ ), and mean separation distance ( $D$ ) of Ag islands on two ZnO samples, with 1000 or 300 Å domain sizes, as a function of deposited amount.

the binding energies of a single metal atom, associated with specific adsorption sites.<sup>31–35</sup> A few calculation schemes have been tested for the adsorption of small metallic clusters.<sup>36,37</sup> Our experimental findings draw attention towards the key role that might be played, in the general context of the VW growth (weak interface adhesion energy or strong differences in surface free energies) as well as concerning the metal-oxide adhesion process, by adsorbate-oxide interactions over a large scale (26–100 Å in the Ag/ZnO case).

### E. The influence of the ZnO-Zn crystalline order on islands morphology

As for the interplay between ZnO crystalline order and metal nucleation growth, it has been further investigated by x-ray scattering at small angles near (0,0). Figure 7(a) shows a typical 2D intensity pattern recorded by use of a CCD camera (56.25  $\mu\text{m}$  pixel size), placed perpendicular to the surface plane and to the incident x-ray beam, at 1680 mm downstream of the sample. The image corresponds to 12 Å of silver on a ZnO-Zn surface with a CDS of 1000 Å (sample labeled as A1000). The active window angular apertures were 2.2° parallel to the surface ( $y$  axis) and 2.4° perpendicular to it ( $z$  axis), corresponding to a range of values, between  $-1.75$  and  $1.75 \text{ nm}^{-1}$  for  $q_y$  and between 0 and  $3.8 \text{ nm}^{-1}$  for  $q_z$ . Intensity profiles, either parallel to the surface [ $I(q_y)$  at fixed  $q_z$ ], or perpendicular to it [ $I(q_z)$  at fixed  $q_y$ ], were first extracted from the 2D intensity patterns. Selected profiles for different amounts of Ag on sample A1000 are shown in Figs. 7(b) and 7(c). The simulation is based on

TABLE I. Morphological parameters derived from the GISAXS intensities for different amounts of Ag on ZnO(0001)-Zn and for two surface coherent domain size (CDS) values. A paracrystal model of cylinderlike islands was used.  $R$ ,  $H$ ,  $D$ ,  $\omega$ , are the in-plane radius, height, interisland mean distance, and separation fluctuation, respectively. The island height-to-width ratio ( $H/2R$ ) and surface coverage ( $\Theta$ ) are also indicated.

Ag (Å)	$2R$ (Å)	$H$ (Å)	$D$ (Å)	$\omega$ (Å)	$H/2R$	$\Theta$
ZnO(0001)-Zn face with a CDS of 1000 Å						
3	22.4	10.7	37.8	26.4	0.48	0.27
6	34.6	11.9	58.4	20.9	0.34	0.27
12	53.0	14.7	92.3	30.7	0.28	0.26
ZnO(0001)-Zn face with a CDS of 300 Å						
2	21.4	13.3	40.0	19.1	0.62	0.22
4	23.2	13.2	56.0	17.9	0.57	0.14
6	32.6	16.3	63.8	18.5	0.50	0.10
8	38.0	17.0	79.2	24.0	0.45	0.18
10	44.4	17.3	95.9	29.3	0.39	0.17
14	54.6	19.6	126.0	37.7	0.36	0.15

a paracrystal-like distribution of scattering entities, which are isolated islands in the early growth stages.<sup>38,39</sup> The fit parameters are the island average in-plane size  $2R$ , height  $H$ , mean separation distance  $D$ , and paracrystal fluctuation  $\omega$ . Details on the GISAXS analysis are given in a recent paper (Ref. 11) which focuses on the differences in Ag island morphology and growth mode according to the surface termination (O or Zn). A simple model of cylinderlike islands allows an almost perfect simulation of the GISAXS intensities for sample A1000. We compare in Table I [Fig. 7(d)] the  $2R$ ,  $H$ ,  $D$ ,  $\omega$  values obtained in the 0–14 Å coverage range to those obtained from a sample (A300) with a CDS of 300 Å. In this latter case, triangular islands with an in-plane size distribution should be considered rather than cylinders in the 8–14 Å coverage range to feature out the whole scattering.<sup>11</sup> However, as we only aim here at demonstrating that a high ZnO crystalline order enhances the 2D shape of the islands as well as the surface covering, the analysis was restricted to the cylinder model.

First, in the nominal thickness range under study, the height values for A1000 are lower than for A300, whereas the  $2R$  values are slightly higher, the height-to-width ratio  $H/2R$  decreasing from 0.48 to 0.28 for A1000 and from 0.595 to 0.375 for A300. The plateau island shape is thus significantly enhanced using a long-range ordered template. The second noticeable result is the reduction of the interisland distance in sample A1000 with respect to A300, indicating the fraction of the surface covered by silver is higher (see the parameter  $\Theta \sim \pi R^2/D^2$ , which accounts for the local island area coverage). Growth proceeding by diffusion-mediated aggregation<sup>40–42</sup> results in a strong correlation between island size and separation. The proportionality factor between the nearest-neighbor distance  $D$  and the width  $2R$  is 1.75 for A1000, in comparison of 2.2 for A300. The mobility of adatoms or nucleated entities is favored on the surface A1000, leading to a higher island density and a lower island

size distribution. Indeed, for that surface, the diffuse intensity is highly concentrated towards  $q_y \sim 2\pi/D$  at any coverage [see the rodlike signal in Fig. 7(a)]. Surface structural defects, by blocking some adatoms or some small clusters, may inhibit the growth of precursor islands on top of terraces. The ZnO-Zn surface being stabilized by triangular holes and protuberances,<sup>17,43</sup> high annealing temperatures presumably induce larger terraces with less pits and protrusions. The high wetting by silver of the ZnO-O surface<sup>11</sup> could also be helped by surface flatness,<sup>10</sup> although the anionic termination is certainly the most important parameter.<sup>32,34</sup>

#### IV. SUMMARY AND CONCLUSION

When long-range order is obtained on basal ZnO surfaces, one observes almost exclusively the Ag(111) epitaxy in which the closest-packed atomic rows of Ag are aligned with those of ZnO. The islands adopt their bulk lattice parameter

(to within  $-0.3\%$ ) from the very beginning of the growth, whereas the interface mismatch is  $-11.1\%$ . The growth in the very first stages is rather lateral, leading to a plateaulike morphology. This is enhanced by improving the surface crystalline order. A faint proportion of Ag islands rotated by  $30 \pm 3^\circ$  in the surface plane is sometimes detected. Their build-up in height [(111) fcc stacking] occurs only on ill-crystallized surfaces and the islands are compressively strained with respect to bulk Ag (up to an amount of  $-2.6\%$ ). The growth is rapidly inhibited with respect to that of fully relaxed islands with  $0^\circ$  orientation. A coincidence superstructure involving 9 (8) Ag (ZnO) unit cells appears as the driving force for the stabilization of the bulklike islands. Such metal-oxide interface superstructures could be used as arrays of selective adsorption sites in catalysis<sup>29</sup> or as templates for nanodots growth. In the field of electronic junctions,<sup>4</sup> one could take advantage of the coherent tunneling conductance at the matching zones.

\*Electronic address: nathalie.jedrecy@insp.jussieu.fr

- <sup>1</sup>V. Koss, A. Belkind, K. Memarzadeh, and J. A. Woollam, *Sol. Energy Mater.* **19**, 67 (1989).
- <sup>2</sup>Z. Xu, F.-S. Xiao, S. K. Purnell, O. Alexeev, S. Kawi, S. E. Deutsch, and B. C. Gates, *Nature (London)* **372**, 346 (1994).
- <sup>3</sup>C. T. Campbell, S. C. Parker, and D. E. Starr, *Science* **298**, 811 (2002).
- <sup>4</sup>S. Yuasa, T. Nagahama, A. Fukushima, Y. Suzuki, and K. Ando, *Nat. Mater.* **3**, 868 (2004).
- <sup>5</sup>G. Renaud, *Surf. Sci. Rep.* **32**, 1 (1998).
- <sup>6</sup>M. Bäumer and H.-J. Freund, *Prog. Surf. Sci.* **61**, 127 (1999).
- <sup>7</sup>J. H. van der Merwe and E. Bauer, *Phys. Rev. B* **39**, 3632 (1989).
- <sup>8</sup>A. D. Novaco and J. P. McTague, *Phys. Rev. Lett.* **38**, 1286 (1977).
- <sup>9</sup>K. H. Ernst, A. Ludviksson, R. Zhang, J. Yoshihara, and C. T. Campbell, *Phys. Rev. B* **47**, 13782 (1993).
- <sup>10</sup>N. Jedrecy, S. Gallini, M. Sauvage-Simkin, and R. Pinchaux, *Phys. Rev. B* **64**, 085424 (2001).
- <sup>11</sup>N. Jedrecy, G. Renaud, R. Lazzari, and J. Jupille, *Phys. Rev. B* **72**, 045430 (2005).
- <sup>12</sup>S. Djanarthany, D. Abriou, R. Lazzari, and J. Jupille (unpublished).
- <sup>13</sup>E. Vlieg, *J. Appl. Crystallogr.* **30**, 532 (1997).
- <sup>14</sup>N. Jedrecy, *J. Appl. Crystallogr.* **33**, 1365 (2000).
- <sup>15</sup>G. Renaud, M. Ducruet, O. Ulrich, and R. Lazzari, *Nucl. Instrum. Methods Phys. Res. B* **222**, 667 (2004).
- <sup>16</sup>N. Jedrecy, M. Sauvage-Simkin, and R. Pinchaux, *Appl. Surf. Sci.* **162-163**, 69 (2000).
- <sup>17</sup>O. Dulub, U. Diebold, and G. Kresse, *Phys. Rev. Lett.* **90**, 016102 (2003).
- <sup>18</sup>I. K. Robinson, *Phys. Rev. B* **33**, 3830 (1986).
- <sup>19</sup>J. M. Zuo and B. Q. Li, *Phys. Rev. Lett.* **88**, 255502 (2002).
- <sup>20</sup>Y. Liu, Y. G. Cao, H. S. Wu, M. H. Xie, and S. Y. Tong, *Phys. Rev. B* **71**, 153406 (2005).
- <sup>21</sup>C. T. Campbell, *Surf. Sci. Rep.* **27**, 1 (1997).
- <sup>22</sup>P. Liu, Y. W. Zhang, and C. Lu, *Phys. Rev. B* **68**, 035402 (2003).
- <sup>23</sup>J. Drucker, *Phys. Rev. B* **48**, 18203 (1993).
- <sup>24</sup>J. K. Bording, B. Q. Li, Y. F. Shi, and J. M. Zuo, *Phys. Rev. Lett.*

- 90**, 226104 (2003).
- <sup>25</sup>C. Günther, J. Vrijmoeth, R. Q. Hwang, and R. J. Behm, *Phys. Rev. Lett.* **74**, 754 (1995).
- <sup>26</sup>I. Meunier, G. Tréglia, J.-M. Gay, B. Aufray, and B. Legrand, *Phys. Rev. B* **59**, 10910 (1999).
- <sup>27</sup>H. C. Galloway, P. Sautet, and M. Salmeron, *Phys. Rev. B* **54**, R11145 (1996).
- <sup>28</sup>Sh. Shaikhutdinov, M. Ritter, and W. Weiss, *Phys. Rev. B* **62**, 7535 (2000).
- <sup>29</sup>C. Castellarin-Cudia, S. Surnev, G. Schneider, R. Podlucky, M. G. Ramsey, and F. P. Netzer, *Surf. Sci.* **554**, L120 (2004).
- <sup>30</sup>J. Gustafson, A. Mikkelsen, M. Borg, E. Lundgren, L. Köhler, G. Kresse, M. Schmid, P. Varga, J. Yuhara, X. Torrelles, C. Quirós, and J. N. Andersen, *Phys. Rev. Lett.* **92**, 126102 (2004).
- <sup>31</sup>A. Bogicevic and D. R. Jennison, *Phys. Rev. Lett.* **82**, 4050 (1999).
- <sup>32</sup>B. Meyer and D. Marx, *Phys. Rev. B* **69**, 235420 (2004).
- <sup>33</sup>Y. F. Zhukovskii, E. A. Kotomin, B. Herschend, K. Hermansson, and P. W. M. Jacobs, *Surf. Sci.* **513**, 343 (2002).
- <sup>34</sup>J. R. B. Gomes, F. Illas, N. C. Hernández, A. Márquez, and J. F. Sanz, *Phys. Rev. B* **65**, 125414 (2002).
- <sup>35</sup>L. Giordano, J. Goniakowski, and G. Pacchioni, *Phys. Rev. B* **64**, 075417 (2001).
- <sup>36</sup>W. Vervisch, C. Mottet, and J. Goniakowski, *Phys. Rev. B* **65**, 245411 (2002).
- <sup>37</sup>A. Eichler, *Phys. Rev. B* **68**, 205408 (2003); **71**, 125418 (2005).
- <sup>38</sup>R. Lazzari, *J. Appl. Crystallogr.* **35**, 406 (2002).
- <sup>39</sup>A program dedicated to GISAXS analysis may be downloaded from: [http://www.esrf.fr/computing/scientific/joint\\_projects/IsGISAXS](http://www.esrf.fr/computing/scientific/joint_projects/IsGISAXS) (2002)
- <sup>40</sup>M. C. Bartelt, A. K. Schmid, J. W. Evans, and R. Q. Hwang, *Phys. Rev. Lett.* **81**, 1901 (1998).
- <sup>41</sup>M. C. Bartelt, C. R. Stoldt, C. J. Jenks, P. A. Thiel, and J. W. Evans, *Phys. Rev. B* **59**, 3125 (1999).
- <sup>42</sup>E. Cox, M. Li, P.-W. Chung, C. Ghosh, T. S. Rahman, C. J. Jenks, J. W. Evans, and P. A. Thiel, *Phys. Rev. B* **71**, 115414 (2005).
- <sup>43</sup>T. M. Parker, N. G. Condon, R. Lindsay, F. M. Leibsle, and G. Thornton, *Surf. Sci.* **415**, L1046 (1998).